Enhanced Thermal Decomposition and Laser Ignition Properties of Nanostructured NC/Al/RDX Composite Fibers Fabricated by Electrospinning

Weimin Wang
Northwest University
Hui Li
Xi'an Modern Chemistry Research Institute
Yanjing Yang
Xi'an Modern Chemistry Research Institute
Fengqi Zhao
Xi'an Modern Chemistry Research Institute
Heng Li
Xi'an Modern Chemistry Research Institute
Kangzhen Xu (antiquake@163.com)
Northwest University https://orcid.org/0000-0002-1362-4213

Research Article

Keywords: electrospinning, nano-aluminum, nanocomposite fibers, thermal behavior, laser ignition

Posted Date: February 12th, 2021

DOI: https://doi.org/10.21203/rs.3.rs-184430/v1

Abstract

Nano Al has always been the research hotspot in the field of energetic materials because of its high energy density and combustion temperature, and has been considered as a fuel to enhance the energy release of various propulsive systems. In this work, nanocomposite fibers were fabricated by electrospinning technology, in which nano Al and recrystallized RDX particles were integrated with NC fibers. The morphology and chemical components of NC/Al, NC/RDX, and NC/Al/RDX composite fibers were characterized by XRD, FT-IR, SEM, TEM and BET. The agglomeration of nano Al particles in fibers is significantly inhibited, and the recrystallized RDX and nano Al particles are uniformly dispersed in NC fibers, resulting in the rough surfaces of the composite fibers. The thermal analysis shows that nano NC fibers have lower thermal decomposition temperature (202.1 ℃) and apparent activation energy (149.32 kJ mol^{-1}) than raw NC (208.2 ℃ and 218.5 kJ mol^{-1}), and NC/Al/RDX exhibits improved thermal decomposition properties compared with NC/RDX and NC/Al. The laser ignition experiments suggest that the uniformly dispersed nano Al particles could obviously promote the combustion and shorten ignition delay time. However, RDX may delay ignition due to its high decomposition temperature, but can significantly enhance the combustion properties of NC/Al/RDX fibers. Among the all samples, the NC/Al/RDX (1:1:0.2) exhibits shortest ignition delay time and most violent combustion flames, which can be attributed to the fibrous structure and the enhanced heat and mass transfer between the components.

1. Introduction

Energetic materials (EMs) are widely used in both civilian and military fields (Dai et al. 2018a; Ahn and Kim 2017). Propellants, as an important branch of EMs, are the main power source of rocket and missile motors (Wang et al. 2020). Solid propellants, which are generally composed of high-energy oxidants, fuels, binders, curing agents and other functional additives, can be classified into homogeneous (double-based propellants) and heterogeneous (composite modified double-based propellants and composite propellants) propellants according to the structure properties between components (Yan et al. 2020; Liu et al. 2019; Son et al. 2007). Compared with the homogeneous propellants, the heterogeneous propellants generally have higher energy densities because of the existence of metal fuels (like Al and Mg) and high energy oxidants. However, because the thermal decomposition reaction kinetics of solid propellants is dominated by mass transfer and heat diffusion, phase separation in the heterogeneous propellants affects their energy release (Sundaram et al. 2017; Tillotson et al. 2001). To increase interface contact and decrease distances of mass transfer and heat diffusion, nanoscale metal fuels should be selected and mixed with oxidants sufficiently for the heterogeneous propellants (Yan et al. 2012; Wang et al. 2014).

Aluminum (Al) powder is one of the most important components for the heterogeneous propellants, and can significantly improve the energy performance of solid propellants due to its high enthalpy and combustion temperature (Arkhipov et al. 2012; Dokhan et al. 2002). In addition, the ignition temperature of nano Al powder (≈1000 K) is closer to surface temperature of Al-containing propellants (~ 800 K) compared with that of micro Al powder (~ 2300 K). The burning flame of nano Al-containing propellants

is closer to the propellant surfaces compared with that of micro Al-containing propellants, resulting in better heat feedback and higher burning rates (Jian et al. 2013; Young et al. 2015; Pang et al. 2019). However, the application of nano Al powder in propellants still faces some processing challenges. The nano Al powder with small particle size can increase viscosity of polymer binders and is prone to agglomeration, and its pre-reaction sintering can increase the effective size to a micron scale, which limits its large-scale potential applications in formulations (Lebedeva et al. 2012; Lyu et al. 2019; Galfetti et al 2007). Although many approaches, such as self-assembly, sol-gel synthesis and sputtering, were employed to deal with these issues by controlling structure properties and loading of nanoparticles, the sensitivity of materials to heat and sparks increased, thus decreasing their safety (Petrantoni et al. 2010; Calais et al. 2017; Tillotson et al. 2001).

Electrospinning, which is one of the simplest top-down preparation approaches to obtain versatile functional fibers from many polymer systems, is usually applied in the fields of optical devices, biomedical and healthcare products, sensors and filtration and purification for air and water (Yan et al. 2012; Luo et al. 2012; Ding et al. 2010). Nitrocellulose (NC) and cyclotrimethylenetrinitramine (RDX) are a common energetic binder and a high energy oxidizer for propellants, respectively (Jian et al. 2013). In this work, the energetic NC/Al/RDX nanocomposite fibers were prepared by the electrospinning, in which nano Al and recrystallized RDX particles were uniformly dispersed in the NC fibers. Morphology, phase composition, thermal decomposition and laser ignition properties of the NC/Al/RDX nanocomposite fibers were characterized and analyzed. The effects of nano Al and RDX on the ignition delay and combustion properties were studied. The results will lay the foundation for further investigating the combustion properties of NC/Al/RDX and eventually enlarge the application range of this kind of energetic materials in propellants.

2. Experimental Section

2.1 Reagents and materials

All the chemical reagents are commercially available and were directly used as received without further purification. Aluminum nanoparticles (Al NPs) with an average diameter of ~ 100 nm were purchased from Beijing Innochem Technology Co., Ltd. The active aluminum content was determined to be ~ 82 wt.% by thermogravimetry/differential scanning calorimetry (TG/DSC) analysis. NC with the nitrogen content of 11.8–12.1% and RDX were provided by Xi’an Modern Chemistry Research Institute.

2.2 Precursor preparation

Ethanol and acetone were mixed at a volume ratio of 1:1 to form a homogeneous mixture solution. NC was added into the mixture solution at a mass ratio of 1:10 (NC/mixture solution) in each experimental formulation. Typically, for NC/Al/RDX composite fibers, NC was first dissolved in the mixture solution and vigorously stirred for 0.5 h to obtain a NC solution. Then, Al NPs were uniformly dispersed in the NC solution through ultrasonic treatment for 0.5 h. Finally, RDX was added into the above Al /NC solution

and magnetically stirred for 24 h at room temperature. The preparation processes of other precursor solutions for NC/Al, NC/RDX or NC were similar to those depicted above.

2.3 Electrospinning process

The fabrication schematic diagram of composite fibers is shown in Fig. 1. As illustrated, the precursor solution was loaded in a syringe, fed by a syringe pump at a rate of 0.02 mm s^{-1}. A working voltage of 18 kV was attached to the stainless nozzle to create a high electrostatic field. The working distance between nozzle-tip and collector substrate was kept at 22 cm. The products were collected from the aluminum foil which covers the collector substrate at -2 kV static. For safety purposes, all operations were carefully processed in case of electric shock, and the whole experimental processes were carried out in the fume hood.

2.4 Morphology and composition characterization

The surface morphology and microstructure properties of the samples were observed by Field emission scanning electron microscopy (FESEM, Carl Zeiss SIGMA HV) with a working distance of ~ 6 mm at an accelerating voltage of 5 kV. The nanocomposite fibers were adhered to a carbon-tape on an SEM stage and then sputtered with gold using ion sputtering device for the FESEM observation. Transmission electron microscopy (TEM, FEI Tecnai G2 microscope) was employed to characterize the distribution of Al NPs inside the NC fibers at 200 kV. The composition and crystal phase of the nanocomposite fibers were determined by powder X-ray diffraction (XRD, Rigaku Mini Flex 600, Japan) using Cu Kα radiation (λ = 1.5406 Å) at 40 kV voltage and 40 mA current with a scanning rate of 5 ° min^{-1} in the 2θ range from 5 ° to 80 °. Infrared spectra were recorded on a Fourier transform infrared spectrophotometry (FT-IR, Shimadozu IRAffinity-1S WL, Japan) over the range of 400–4000 cm^{-1}. The specific surface areas of nanocomposite fibers were measured using nitrogen adsorption/desorption instrument (Micromeritics ASAP 2460) and calculated by a multipoint Brunauer-Emmett-Teller (BET) method. The samples were degassed at 120 ℃ for 12 h before Nitrogen adsorption.

2.5 Thermal behavior analysis

Differential scanning calorimetry (DSC) was employed to investigate the thermal decomposition properties of NC, RDX and nanocomposite fibers prepared by electrospinning, and performed on a DSC Instrument (Netzsch, 200F3) in a high-purity Nitrogen atmosphere with a flow rate of 20 mL min^{-1} under ambient pressure. About 1 mg samples was used and placed in an alumina crucible for thermal analysis at a heating rate of 10 ℃ min^{-1} from room temperature to 350 ℃.

2.6 Laser ignition tests

The laser ignition properties of the samples were investigated by a carbon dioxide laser ignition system (SLC 110) in air atmosphere. The output power was corrected by an optical power meter before each ignition experiment. The optical emission indicates an ignition event, which could be used to measure the ignition delay time (Dai et al. 2018b). The ignition delay time was defined by the time difference from the triggering of the laser to the initial photo signal of igniting flame. The combustion processes were

recorded by a high-speed digital camera to capture the flame images at a frame rate of 1000 frames per second. For reducing the experimental error, each sample was performed at least three times under the same laser power density, and then the average values were taken to investigate the ignition properties of the samples.

3. Results And Discussion

3.1 Chemical composition and morphology analysis of nanocomposite fibers

XRD patterns of Al, RDX, NC fibers and composite fibers are shown in Fig. 2 **(a)**. For NC/Al and NC/Al/RDX composite fibers, all diffraction peaks of nano Al observed at 2θ = 38.5, 44.6, 65.2 and 78.2° can be indexed to (111), (200), (220) and (311) crystal planes of Al, respectively, which corresponds well with the standard pattern of single Al (JCPDS No. 04-0787). All diffraction peaks of recrystallized RDX in NC/RDX and NC/Al/RDX are well consistent with those of raw RDX, indicating the unchanged crystal phase of recrystallized RDX particles during the electrospinning process. A broad protruding peak can be observed in the XRD pattern of NC fibers due to that NC is a type of energetic polymer (Luo et al. 2019). Contrast to the diffraction peaks of NC fibers and RDX, the intensity of diffraction peaks for NC and RDX in NC/Al and NC/Al/RDX is relatively weak, which is caused by the strong intensity of the diffraction peaks of nano Al. The XRD results suggest that RDX and nano Al particles can be successfully incorporated into NC fibers via electrospinning.

FT-IR spectra of the samples were recorded to explore their surface functional groups, as displayed in Fig. 2 **(b)**. Two strong absorption peaks of NC fibers located at 1629.8 and 1271.0 cm^{-1} can be assigned to the symmetric and anti-symmetric stretching vibrations of -ONO_2, respectively. The characteristic peaks observed at 821.7, 995–1056 and 670–745 cm^{-1} are attributed to the deformation vibration of C-O-NO_2, the inter-ring stretching vibration of C-O and the scissoring and rock vibrations of -NO_2, respectively. All these absorption peaks match well with the molecular structure of NC (Luo et al. 2020; Ma Angeles et al. 2011). In composite fibers, the FT-IR characteristic absorption peaks of NC are consistent with those of NC fibers, but their intensity changes slightly, indicating that the structure of polymer molecules did not change during the electrospinning process. For the FT-IR spectrum of RDX, the absorption peaks located at 1531.5 and 1570.1 cm^{-1} are assigned to the asymmetric stretching vibrations of -ONO_2. The peaks located at 1458 and 1421 cm^{-1} are related to CH_2 deformation vibrations in the ring of RDX molecule. The peaks located at 1384, 1200, 782.5 and 588.9 cm^{-1} are ascribed to the symmetric stretching vibrations of -NO_2, the stretching vibrations of N-NO_2, the deformation vibration and stretching vibration of -NO_2, respectively. The absorption peaks of the bending vibrations of the RDX ring can be found at 1037.7 and 908.5 cm^{-1} (Chen et al. 2019; Gao et al. 2017; Carlos et al. 2010). In the spectra of both NC/RDX and NC/Al/RDX, the positions of characteristic absorption peaks of the recrystallized RDX particles are roughly same with those of RDX, but their intensity is significantly weakened due to the low

content of RDX in composite fibers. Thus, based on the above analysis, the recrystallized RDX particles were successfully merged in NC fibers.

Optical images of nonwoven nanofiber mats prepared by electrospinning are shown in Fig. 3. For nanocomposite fibers, the nonwoven mats with different composition show different colors, and the colors change from white for NC/RDX to gray for NC/Al/RDX and black for NC/Al, because of the addition of nano Al particles. The pure NC fiber and NC/RDX composite nanofiber mats present the same color. The nanofiber mats with different composition can be obtained through the appropriate selection of solvent.

Figure 4 shows SEM images of RDX, nano Al and NC before and after electrospinning. RDX particles are ellipsoids with diameters of 4–10 μm. There are obvious cracks on the surface of the particles, which could be unfavorable for improving the sensitivity of RDX crystals. The average diameter of nano Al particles is about 100 nm. Figure 4 **(c)** and **(d)** reveal the surface morphology and structural characteristics of NC before and after electrospinning. Before electrospinning, NC presents as short and thick fibers with a diameter of about 20 μm and has a rough and irregular surface morphology. However, after processed, well-defined interconnected networks constructed by NC fibers are obtained, and the insert shows that the NC fibers have smooth surfaces and an average diameter of about 1 μm.

The microstructure and surface morphology of the composite fibers with different composition were characterized by SEM and shown in Fig. 5. In Fig. 5 **(a)-(a")**, the recrystallized RDX particles during the electrospinning process are tightly adhered to the surfaces of NC fibers, and the composite fibers present a rough surfaces and uneven diameter distribution. It should be noted that with the decrease of RDX, the diameters and surfaces of NC/RDX fibers gradually become more uniform and smoother, and the beadlike structures in NC/RDX nanofiber mats decrease. The morphology differences between NC/RDX and NC fibers are mainly caused by two factors. One is that the addition of RDX nanoparticles leads to the inhomogeneity of the precursor solution. The other is that partial recrystallized RDX particles agglomerate to form the beadlike structures during the electrospinning process. SEM images indicate that RDX particles tightly loading on NC fibers have a significantly effect on the surface morphology and structure of the composite fibers.

Figure 5 **(b)-(b") and (c)-(c")** show SEM images of NC/Al and NC/Al/RDX via electrospinning. Uniform and well-defined interconnected fibrous networks can be observed in all the six composite samples. It is remarkable that when nano Al content in the composite fibers is high, such as NC/Al with mass ratio of 1:1 in Fig. 5 **(b)**, the obtained NC/Al fibers have rough and irregular surface morphology compared with NC fibers, which may be accused by the increased viscosity of the precursor solutions due to the addition of excess nano Al power and the agglomeration of nano Al particles during the electrospinning process. Moreover, the inhomogeneous of precursor polymer solution of the composite fibers is caused by the addition of excess nano Al. The composite fibers with low mass loading of Al particles show less obvious aggregation and have relatively smoother surfaces compared with the fibers in Figs. 5 **(b) and (c")**. By comparing NC/Al and NC/Al/RDX, it can be found that NC/Al and NC/Al/RDX present insignificant

differences in fiber surface morphology and diameters, which is because the addition of nano Al particles increases the electrical conductivity of the precursor solution. Thus, compared with RDX, nano Al presents predominant influence on the morphology characteristics of composite fibers. Smaller recrystallized RDX particles in NC/Al/RDX fibers can also be observed **in** Fig. 5 **(a)-(a")**. Moreover, the excess addition of RDX can mess the texture of precursor solution, resulting in the composite fibers with poor morphology.

TEM images of nano Al particles and NC/Al composite fibers with different mass ratio of NC to Al are shown in Fig. 6. Nano Al particles with smooth surfaces and an average diameter of about 100 nm are covered by oxide caps with a thickness of about 5.8 nm, as shown in Fig. 6 **(a)**. Figure 6 **(b-d)** shows that NC/Al composite fibers loaded by nano Al with different contents have quite clear boundaries, and nano Al particles are uniformly incorporated inside the NC fibers and well dispersed, especially for NC/Al with a low nano Al content. When the content of nano Al particles is high in NC/Al [Fig. 6 **(b)**], nano Al particles display more vigorous aggregations inside the fibers. Thus, the surfaces of the composite fibers with a high nano Al content is rougher than those with a low nano Al content, which is consistent with the above SEM results.

BET analysis was performed to further investigate specific surface areas and porous nature of the nanofiber mats prepared by electrospinning. The nitrogen adsorption-desorption isotherms of NC, NC/Al, NC/RDX and NC/Al/RDX composite fibers are shown in Fig. 7. The insert in Fig. 7 presents the pore size distribution of the corresponding samples. The NC fibers have a relatively small specific surface area of about 6.22 $m^2 g^{-1}$. However, after nano Al and RDX particles are incorporated into NC fibers, the specific surface areas of NC/Al, NC/RDX and NC/Al/RDX increase enormously and reach 30.42, 18.32 and 23.26 $m^2 g^{-1}$, respectively. In addition, compared with NC fibers, the pore size distribution of the composite fibers is narrower than that of NC fibers as shown in the inset. The larger specific surface areas and narrower pore size distribution of NC/Al, NC/RDX and NC/Al/RDX can be attributed to the uniform distribution of nano Al and recrystallized RDX particles in the NC fibers and their rough surfaces.

3.2 Thermal properties analysis

The thermal behaviors of the samples were investigated by DSC in Fig. 8. The kinetic parameters of thermal decomposition were calculated by Kissinger and Ozawa methods with the DSC data at different heating rates (5, 10, 15 and 20 ℃ min^{-1}), as listed in Table 1 (Ozawa 1970; Zhang et al. 2020). The thermal decomposition temperature and apparent activation energy of NC fibers are 202.1 ℃ and 149.32 kJ mol^{-1}, respectively, and are significantly lower than those of raw NC (208.2 ℃ and 218.5 kJ mol^{-1}), indicating that nanoization of NC can promote its thermal decomposition. For NC/Al [Fig. 8 **(b)**], especially to NC/Al with the mass ratio of 1:1 (208.5 ℃ and 319.42 kJ mol^{-1}), their thermal decomposition temperature and apparent activation energy are higher than those of NC fibers. The reason is that nano Al particles act as the energy absorber to absorb part of the heat during the heating process, thus delaying the decomposition of NC fibers. The thermal decomposition of NC/RDX exhibits two-stage exothermic processes in Fig. 8 **(c)**, corresponding to two obvious exothermic peaks located at about 206 and 237 ℃ from the exothermic decomposition of NC and RDX, respectively. Compared with

RDX, no melting peak of RDX exists at about 205 ℃ on DSC curves of NC/RDX, which may be because the strongly exothermic decomposition peak of NC covers the weakly melting endothermic peak of RDX. The DSC results indicate that RDX particles are successfully incorporated into the NC fibers with unchanged exothermic behaviors, and the NC decomposes prior to the decomposition of RDX without any intermediate reaction between NC and RDX. Moreover, as shown in Table 1, the thermal decomposition kinetic calculations show that with the increase of NC content in NC/RDX, the apparent activation energy of NC decreases, which is beneficial to promote the ignition of NC/RDX. Figure 8 **(d)** shows that the thermal decomposition peaks of NC and RDX appear simultaneously in NC/Al/RDX, and NC in NC/Al/RDX has lower decomposition temperature than that in NC/RDX and NC/Al. In addition, DSC curve of NC/Al/RDX (1:1:0.2) is similar to that of NC/Al (1:1) due to the low content of RDX. Meanwhile, the apparent activation energy of NC and RDX in NC/Al/RDX (3:1:1) (242.32 and 141.76 kJ mol^{-1}) is higher than those in the NC/Al/RDX (5:1:1) (202.57 and 133.08 kJ mol^{-1}). Thus, NC/Al/RDX (5:1:1) exhibits the enhanced thermal decomposition performances, which is consistent with the short ignition delay time of NC/Al/RDX (5:1:1) during the laser ignition experiments.

Table 1
The kinetic parameters of NC and RDX in different samples obtained by Kissinger and Ozawa Methods.

Samples	Component	Kissinger method			Ozawa method	
		E_k (kJ mol^{-1})	logA (s^{-1})	r	E_o (kJ mol^{-1})	r
Raw NC	NC	218.5	21.99	0.9913	215.65	0.9919
NC-Fibers		149.32	14.47	0.9861	149.54	0.9874
Raw RDX	RDX	177.14	16.11	0.9898	176.56	0.9906
NC/Al (1:1)	NC	319.42	33.42	0.9997	311.3	0.9997
NC/Al (3:1)		226.91	22.97	0.9844	223.37	0.9854
NC/Al (5:1)		174.24	17.04	0.997	173.32	0.9972
NC/RDX (1:1)	NC	188.04	18.67	0.9948	186.4	0.9952
	RDX	149.98	13.46	0.9978	150.66	0.9980
NC/RDX (3:1)	NC	183.72	18.24	0.9908	182.26	0.9915
	RDX	158.32	14.30	0.9984	158.61	0.9986
NC/RDX (5:1)	NC	175.33	17.27	0.9936	174.31	0.9941
NC/Al/RDX (3:1:1)	NC	242.32	24.87	0.9949	237.98	0.9952
	RDX	141.76	12.42	0.9891	142.96	0.9902
NC/Al/RDX (5:1:1)	NC	202.57	20.39	0.9803	200.18	0.9818
	RDX	133.08	11.43	0.9771	134.71	0.9797
NC/Al/RDX (1:1:0.2)	NC	154.71	14.9	0.9983	154.75	0.9985

3.3 Laser ignition properties of energetic nanocomposite fibers

The ignition delay time was measured as a function of the laser power density for NC/Al (a), NC/RDX (b) and NC/Al /RDX (c) composite fibers [Fig. 9 **(a)-(c)**]. The comparison between different composite fibers is presented in Fig. 9 **(d)**. For all composite fibers, the ignition delay time gradually decreases with the increase of laser power density at low laser power density (≤ 200 W cm^{-2}). However, when the laser power density exceeds 200 W cm^{-2}, the ignition delay time almost remains constant and reaches the minimum. For NC/Al, NC/RDX and NC/Al/RDX, the ignition delay time decreases from about 55, 140, and 80 ms at 17.38 W cm^{-2} to about 23, 30, and 24 ms at 250 W cm^{-2}, respectively. The ignition delay time

of NC/Al and NC/Al /RDX is shorter than that of NC/RDX due to the incorporation of nano Al, which indicates that nano Al can shorten the ignition delay time.

The insert in Fig. 9 **(a)** shows that both nano-Al and NC fibers have longer ignition delay time compared to NC/Al at low laser power density, and the ignition delay time of nano Al is larger than that of NC fibers, which may be related to the high melting temperature (~ 2070 ℃) of the oxide cap on the surfaces and the aggregation of nano Al particles. Meanwhile, the larger heat loss rate relative to the energy release rate is also detrimental to the ignition of nano Al (Yan et al. 2020). After incorporating nano Al into NC fibers, the ignition delay time of NC/Al is significantly shortened. Meanwhile, in the same laser power density, the higher content of NC results in shorter the ignition delay time, which is most likely due to the following two factors. First, when the content of nano Al is low, the nano Al particles are evenly dispersed in the NC fibers, and the agglomeration between the particles is significantly restrained by NC, which can be proved by SEM and TEM images of NC/Al. During the laser ignition process, nano Al particles uniformly dispersed in NC act as the major laser energy absorber, which can accelerate the heat diffusion rate from nano Al to NC, thereby shortening the ignition delay time. Second, at the low nano Al content, nano Al particles are mainly dispersed inside the NC fibers, forming NC/Al with structure similar to nested core-shell structure. The NC coating on the surfaces of NC/Al can effectively improve the energy absorption efficiency and prevent the heat diffusion [4]. Figure 9 **(b)** shows that NC/RDX composites present longer ignition delay time than NC, and with the increase of RDX content, the ignition delay time of the composite fibers increases. The characteristic that the ignition delay time of NC/RDX varies with the RDX content may be attributed to the higher thermal decomposition temperature of RDX (~ 242 ℃) than that of NC (~ 208 ℃), resulting in the more energy absorbed by NC/RDX during the laser ignition, so RDX particles have the effect of delaying ignition on NC/RDX. In addition, the recrystallized RDX particles have fewer surface defects, reducing the generation of hot spots, which may also have a certain effect on the ignition delay time of NC/RDX.

It can be seen from Fig. 9 **(c)** that when the laser power density is low, the ignition delay time of NC/Al/RDX (3:1:1) is lightly longer than that of NC, while the ignition delay time of NC/Al/RDX (5:1:1) with a high NC content is below that of NC. The ignition delay time of both NC/Al/RDX (3:1:1) and NC/Al/RDX (5:1:1) are lower than that of NC/RDX composite fibers, which suggests that when nano Al and RDX co-exist in NC/Al/RDX, the promotion effect of nano Al on the ignition delay time of NC is more dominant than the inhibition effect of RDX. This may be related to the high dispersion properties of nano Al and the larger laser energy absorption coefficient than that of RDX (Yan et al. 2020). The characteristic curve of the ignition delay time for NC/Al/RDX (1:1:0.2) also proves the above results, that is, the low content of RDX can shorten the ignition delay. For the composite fibers with different components [Fig. 9 **(d)**], the order of ignition delay time is nano Al □ NC/ RDX (3:1) □ NC/Al/RDX (3:1:1) □ NC fibers □ NC/Al (3:1) at low laser power density. When the laser power density increases, the ignition delay time of NC/RDX (3:1) is still larger than that of other fibers, which further indicates that RDX has a retarding effect on the laser ignition process of the composite fibers.

The combustion processes of nano Al, NC/Al (1:1), and NC/Al/RDX (1:1:0.2) were captured with a high-speed camera during the laser ignition experiments at the laser power density of 200 W cm^{-2}, and the corresponding snapshots are shown in Fig. 10. The burning snapshots of nano Al show that the flame size and shape remain small and constant during the whole burning process, the combustion residues remain as an intact structure. In addition, nano Al has the longer ignition delay time and combustion duration compared with NC/Al (1:1) and NC/Al/RDX (1:1:0.2). The time-consuming of the entire burning process for nano Al is about 7-fold of NC/Al (1:1) and NC/Al/RDX (1:1:0.2). These may be attributed to the high melting temperature (about 2070 ℃) of the oxide cap on the nano Al surfaces and the aggregation of Al nanoparticles, which is consistent with the previous SEM and TEM analysis.

Comparing with nano Al, in addition to the obviously shortened ignition delay and burning time, the shape and size of flame for NC/Al (1:1) and NC/Al/RDX (1:1:0.2) also present significant differences. When NC/Al (1:1) and NC/Al/RDX (1:1:0.2) were ignited, an obvious flame with a great number of twinkling sparks appeared, which then steadily propagated in the radial and axial directions. These bright flames can be roughly divided into central high temperature zone and outer low temperature zone, as distinguished by the brightness. The central high temperature zone is mainly caused by the solid burning residues ejected from the combustion of nano Al dispersed in the composite fibers, while the outer low temperature zone is principally caused by the gas products from the high temperature decomposition of NC and RDX particles. In addition, although the ignition delay time of NC/Al/RDX (1:1:0.2) at the same laser power density (200 W cm^{-2}) is slightly longer than that of NC/Al (1:1), the combustion flames of NC/Al/RDX (1:1:0.2) are brighter and more violent with more sparks splashing out to the ambient and stronger light emission. The flames of NC/Al/RDX (1:1:0.2) consist of stochastic bright spots which were emanated by combustion residues of the nano Al particles, which are much larger and brighter than those of NC/Al (1:1). The larger and brighter flames imply enhanced heat convection and feedback from nano Al particles to ambient gases, which may contribute to the improvement of combustion reactions.

Among nano Al, NC/Al (1:1), and NC/Al/RDX (1:1:0.2), the combustion flames of NC/Al/RDX (1:1:0.2) are the most violent, which are mainly due to the addition of a small amount of RDX. Introducing a few RDX into NC/Al makes NC/Al/RDX (1:1:0.2) deflagrate rapidly after the ignition. This is because the nano Al particles dispersed in the fibers act as the main laser energy absorber and firstly react with NC to release gases and heat, which promotes the ignition of RDX. As a good gas generator, the recrystallized RDX particles rapidly decompose and further release a large quantity of gases and heat. The enormous gaseous products from RDX and NC in the system involved in the quickly combustion process can further retard sintering of the nano Al, which promotes the heat transfer dominated by convection to a certain extent, so NC/Al/RDX (1:1:0.2) shows bright and intense burning flames. In summary, the results of the laser ignition experiments further show that the fibrous NC/Al/RDX composites enhance the interface contact of the components and improve heat feedback to ignition during ultra-fast laser irradiation, thus resulting in the enhancement heat release of the composite fibers.

4. Conclusion

In summary, NC/Al, NC/RDX and NC/Al/RDX nanocomposite fibers were successfully fabricated by electrospinning. The investigations on morphology and chemical components indicate that nano Al particles and recrystallized RDX particles are well dispersed in NC fibers, and the agglomeration of nano Al particles is obviously inhibited, which is beneficial to enhance the heat feedback and improve the laser ignition properties of the composite fibers. The ignition delay time of the composite fibers is related to the activation energy of decomposition for NC in the composite fibers. For the composite fibers with the same composition and different NC contents, the smaller activation energy for NC is, the shorter ignition delay of composite fibers becomes. Meanwhile, the composite fibers containing nano Al particles have shorter ignition delay than that of the fibers without nano Al particles, due to the high dispersion and absorption coefficient of nano Al particles, the enhanced interfacial contact extent and the shortened diffusion distance. But RDX retards ignition due to its higher decomposition temperature than that of NC. However, RDX can significantly enhance the combustion of NC/Al/RDX by inhibiting the agglomeration of nano Al particles. In brief, this research is conductive to further understand the combustion process of NC/Al/RDX composite fibers, and electrospinning would be extended to other nanocomposite fibers for eventually enlarging the application range of this class of energetic materials in propellants.

Declarations

Acknowledgements

This investigation received financial assistance from the Foundation of National Defense Key Laboratory.

References

1. Ahn JY, Kim SH (2017) Encapsulation of aluminum nanoparticles within copper oxide matrix for enhancing their reactive properties. Chem Eng J 325: 249–256
2. Arkhipov VA, Korotkikh AG (2012) The influence of aluminum powder dispersity on composite solid propellants ignitability by laser radiation. Combust Flame 159: 409–415
3. Calais T, Bourrier D, Bancaud A, Chabal Y, Estève A, Rossi C (2017) DNA grafting and arrangement on oxide surfaces for self-assembly of Al and CuO nanoparticles. Langmuir 33: 12193–12203
4. Carlos GP, Julibeth MM, Perla BB (2010) Theoretical infrared and terahertz spectra of an RDX/Aluminum complex. J Phys Chem A 114: 2284–2292
5. Chen T, Gou BW, Hao GZ, Gao H, Xiao L, Ke X, Gou SF, Jiang W (2019) Preparation, characterization of RDX/GAP nanocomposites, and study on the thermal decomposition behavior. J Energ Mater 37: 80–89
6. Dai J, Wang F, Ru CB, Xu JB, Wang CA, Zhang W, Ye YH, Shen RQ (2018a) Ammonium perchlorate as an effective additive for enhancing the combustion and propulsion performance of Al/CuO nanothermites. J Phys Chem C 122: 10240–10247

7. Dai J, Xu JB, Wang F, Tai Y, Shen Y, Shen RQ, Ye YH (2018b) Facile preparation of nitrocellulose-coated Al/Bi2O3 nanothermites with excellent energy output and improved electrostatic discharge safety. Mater Design 143: 93–103
8. Ding B, Wang MR, Wang XF, Yu JY, Sun G (2010) Electrospun nanomaterials for ultrasensitive sensors. Mater today 13: 16–27
9. Galfetti L, DeLuca LT, Severini F, Colombo G, Meda L, Marra G (2007) Pre and post-burning analysis of nano-aluminized solid rocket propellants. Aerosp Sci Technol 11: 26–32
10. Gao H, Jiang W, Liu J, Hao GZ, Xiao L, Ke X, Chen T (2017) Synthesis and characterization of a new co-crystal explosive with high energy and good sensitivity. J Energ Mater 35: 490–498
11. Jian GQ, Chowdhury S, Sullivan K, Zachariah MR (2013) Nanothermite reactions: Is gas phase oxygen generation from the oxygen carrier an essential prerequisite to ignition?. Combust Flame 160: 432–437
12. Lebedeva EA, Tutubalina IL, Val'tsifer VA, Strel'nikov VN, Astaf'eva SA, Beketov IV (2012) Agglomeration of the condensed phase of energetic condensed systems containing modified aluminum. Combust Explo Shock+ 48: 694–698
13. Liu B, Wang WM, Wang JJ, zhang Y, Xu KZ, Zhao FQ (2019) Preparation and catalytic activities of CuFe2O4 nanoparticles assembled with graphene oxide for RDX thermal decomposition. J Nanopart Res 21: 1–9
14. Luo CJ, Stoyanov SD, Stride E, Pelan E, Edirisinghe M (2012) Electrospinning versus fibre production methods: from specifics to technological convergence. Chem Soc Rev 41: 4708–4735
15. Luo TT, Wang Y, Huang H, Shang FF, Song XL (2019) An electrospun preparation of the NC/GAP/Nano-LLM-105 nanofiber and its Properties. Nanomaterials 9: 854–869
16. Luo TT, Wang Y, Liu LX, Song XL (2020) Characterization and thermochemical properties of NC/GAP/Nano-TATB electrospinning composite fibers with 3D network structure. Chin J Energ Mater 28: 925–935
17. Lyu JY, Chen SW, He W, Zhang XX, Tang DY, Liu PJ, Yan QL (2019) Fabrication of high-performance graphene oxide doped PVDF/CuO/Al nanocomposites via electrospinning. Chem Eng J 368: 129–137
18. Ma Angeles FO, Maria LL, Mercedes T, Carmen GR (2011) Analytical techniques in the study of highly-nitrated nitrocellulose. Trac-Trend Anal Chem 30: 1740–1755
19. Ozawa T (1970) Kinetic analysis of derivative curves in thermal analysis. J Therm Anal 2: 301–324
20. Pang WQ, Deluca T L, Fan XZ, Wang K, Li JQ, Zhao FQ (2019) Progress on modification of high active aluminum powder and combustion agglomeration in chemical propellants. J Solid Rocket Techno 42: 42–53
21. Petrantoni M, Rossi C, Salvagnac L, Conédéra V, Estève A, Tenailleau C, Alphonse P, Chabal YJ (2010) Multilayered Al/CuO thermite formation by reactive magnetron sputtering: nano versus micro. J Appl Phys 108: 1–5

22. Pourmortazavi SM, Kohsari I, Zandavar H, Koudehi MF, Mirsadeghi S (2019) Electrospining and thermal characterization of nitrocellulose nanofibers containing a composite of diaminofurazan, aluminum nano-powder and iron oxide nanoparticles. Cellulose 26: 4405–4415
23. Son SF, Yetter RA, Yang V (2007) Introduction: nanoscale composite energetic materials. J Propul Power 23: 643–644
24. Sundaram D, Yang V, Yetter RV (2017) Metal-based nanoenergetic materials: synthesis, properties, and application. Prog Energy Combust Sci 61: 293–365
25. Tillotson TM, Gash AE, Simpson RL, Hrubesh LW, Satcher JH, Poco JF (2001) Nanostructured energetic materials using sol-gel methodologies. J Non-Cryst Solids 285: 338–345
26. Wang HY, Jian GQ, Egan GC, Zachariah MR (2014) Assembly and reactive properties of Al/CuO based nanothermite microparticles. Combust Flame 161: 2203–2208
27. Wang JJ, Lian XY, Yan QL, Gao DY, Zhao FQ, Xu KZ (2020) Unusual Cu-Co/GO composite with special high organic content synthesized by an in situ self-assembly approach: Pyrolysis and catalytic decomposition on energetic materials. ACS Appl Mater Interfaces 12: 28496–28509
28. Yan S, Jian GQ, Zachariah MR (2012) Electrospun nanofiber-based thermite textiles and their reactive properties. ACS Appl Mater Interfaces 4: 6432–6435
29. Yan T, Ren H, Liu J, Jiao QJ (2020) Facile preparation and synergetic energy releasing of nano-Al@RDX@Viton hollow microspheres. Chem Eng J 379: 1–9
30. Young G, Wang HY, Zachariah MR (2015) Application of Nano-Aluminum/Nitrocellulose Mesoparticles in Composite Solid Rocket Propellants. Propell Explos Pyrot 40: 413–418
31. Zhang M, Zhao FQ, An T, Yang YJ, Li H, Pan Q, Wang XH, Jiang ZF (2020) Catalytic effects of rGO-MFe2O4 (M = Ni, Co, and Zn) nanocomposites on the thermal decomposition performance and mechanism of energetic FOX-7. J Phys Chem A 124: 1673–1681

Figures

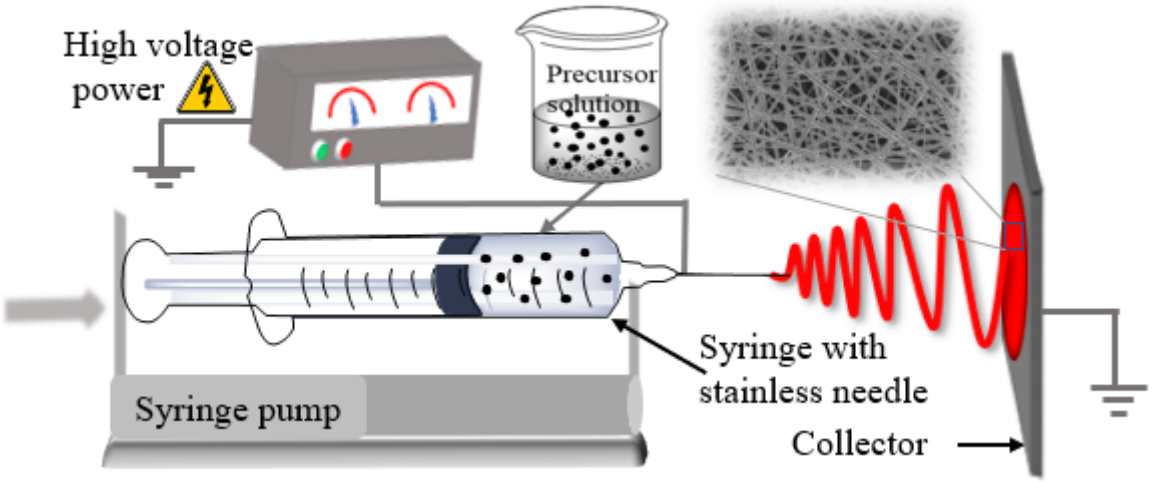

Figure 1

Schematic diagram of nanocomposite fibers fabrication via electrospinning.

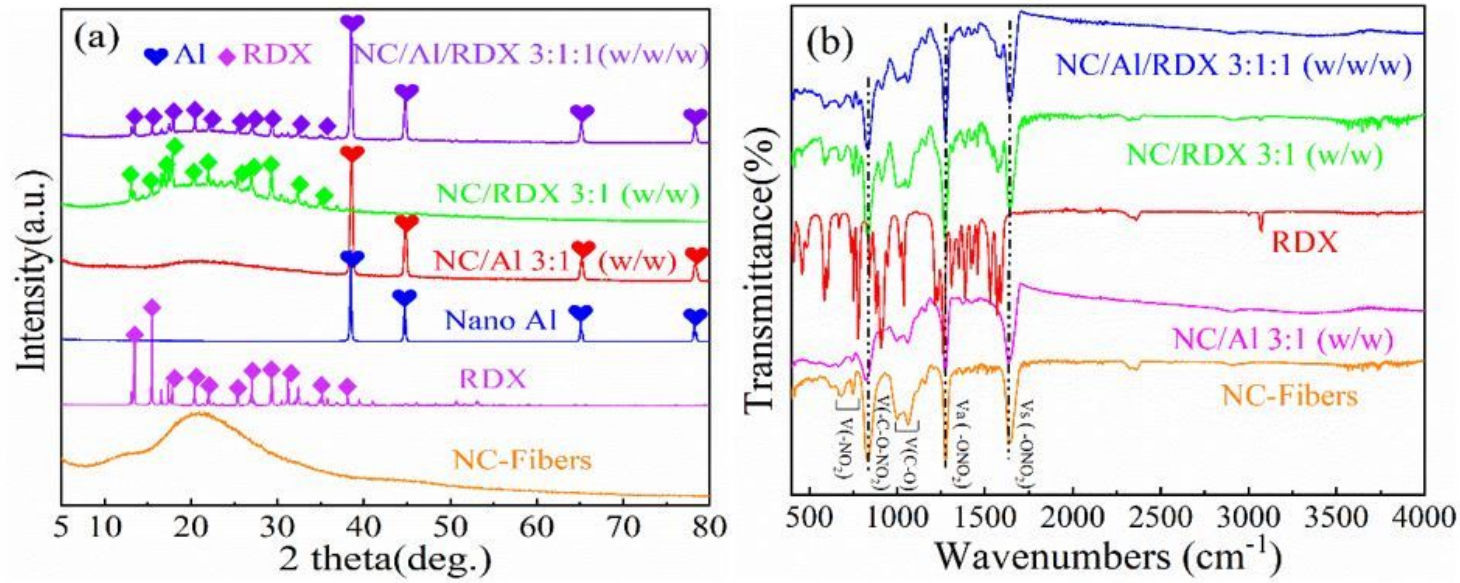

Figure 2

XRD (a) and FT-IR (b) spectra of NC fibers, Al, RDX and nanocomposite fibers

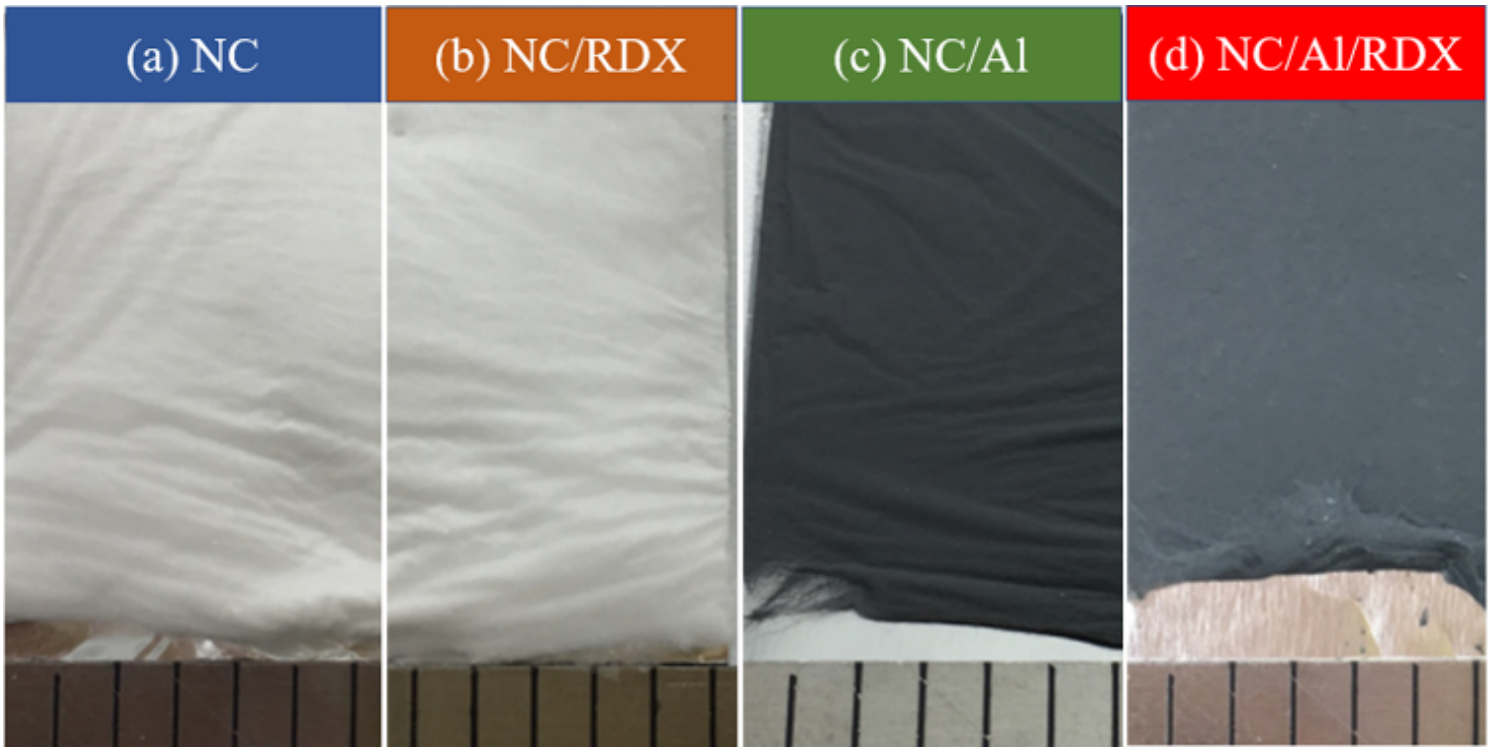

Figure 3

Photographs of nanofiber mats fabricated by electrospinning.

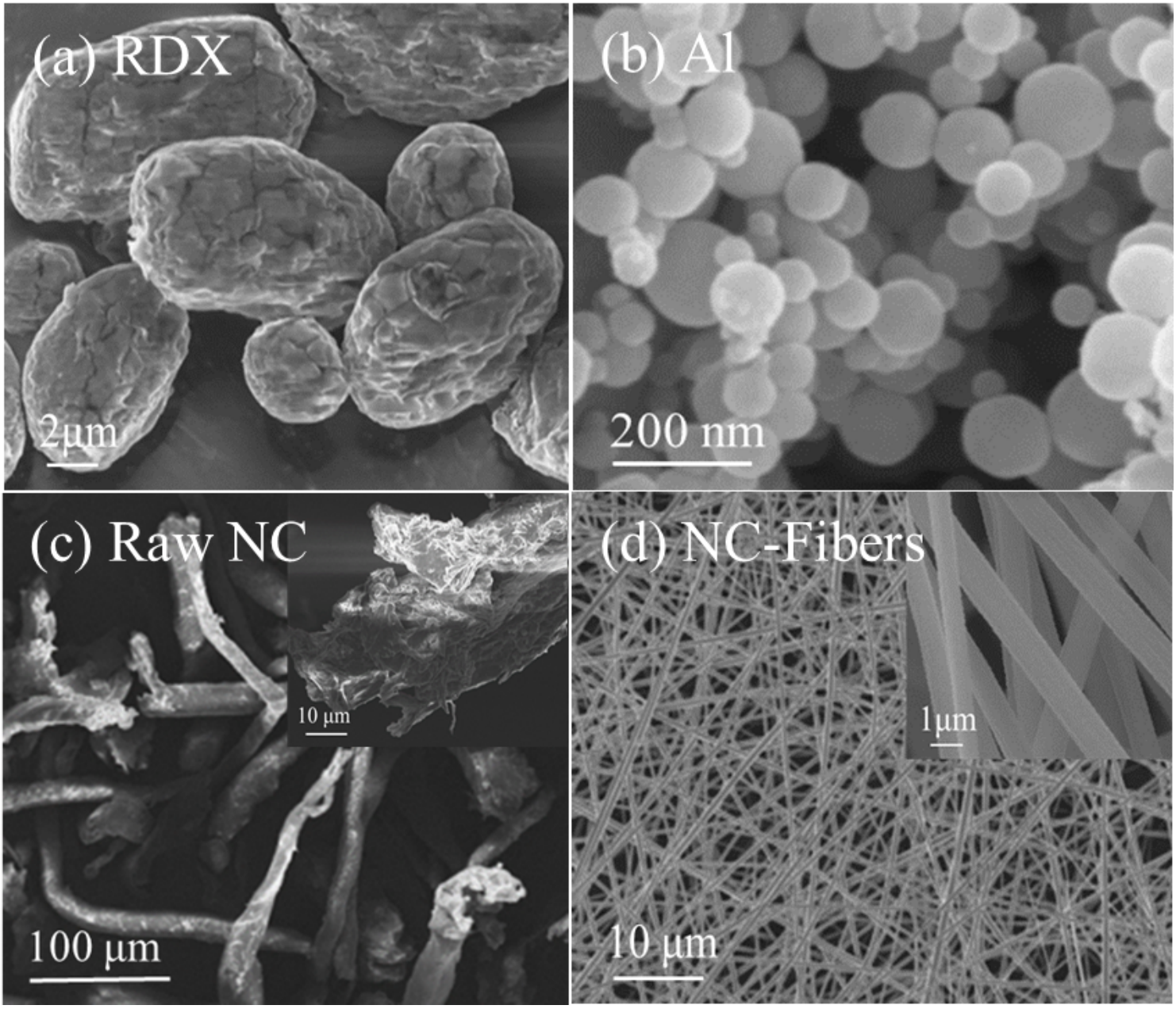

Figure 4

SEM images of RDX (a), nano Al (b), NC (c) and NC nanofibers (d).

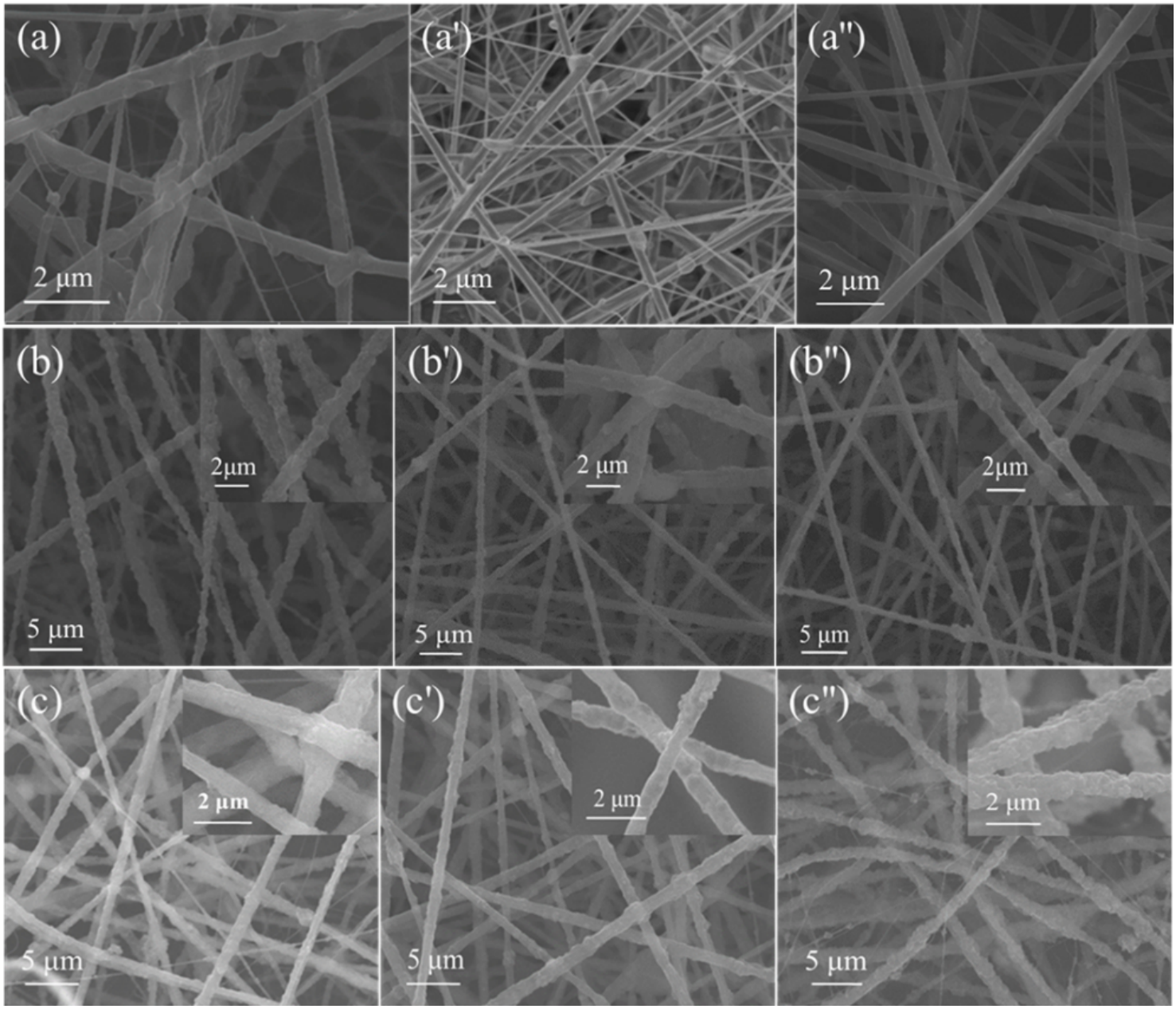

Figure 5

SEM images of NC/RDX (a-a"), NC/Al (b-b") and NC/Al/RDX (c-c") nanofibers. Note: from a (b) to a" (b"), the mass ratio of NC to RDX (Al) is 1:1, 3:1, 5:1, respectively; the mass ratio of NC, Al, RDX is 5:1:1 (c), 3:1:1 (c'), 1:1:0.2 (c") for NC/Al/RDX nanofibers mats, respectively.

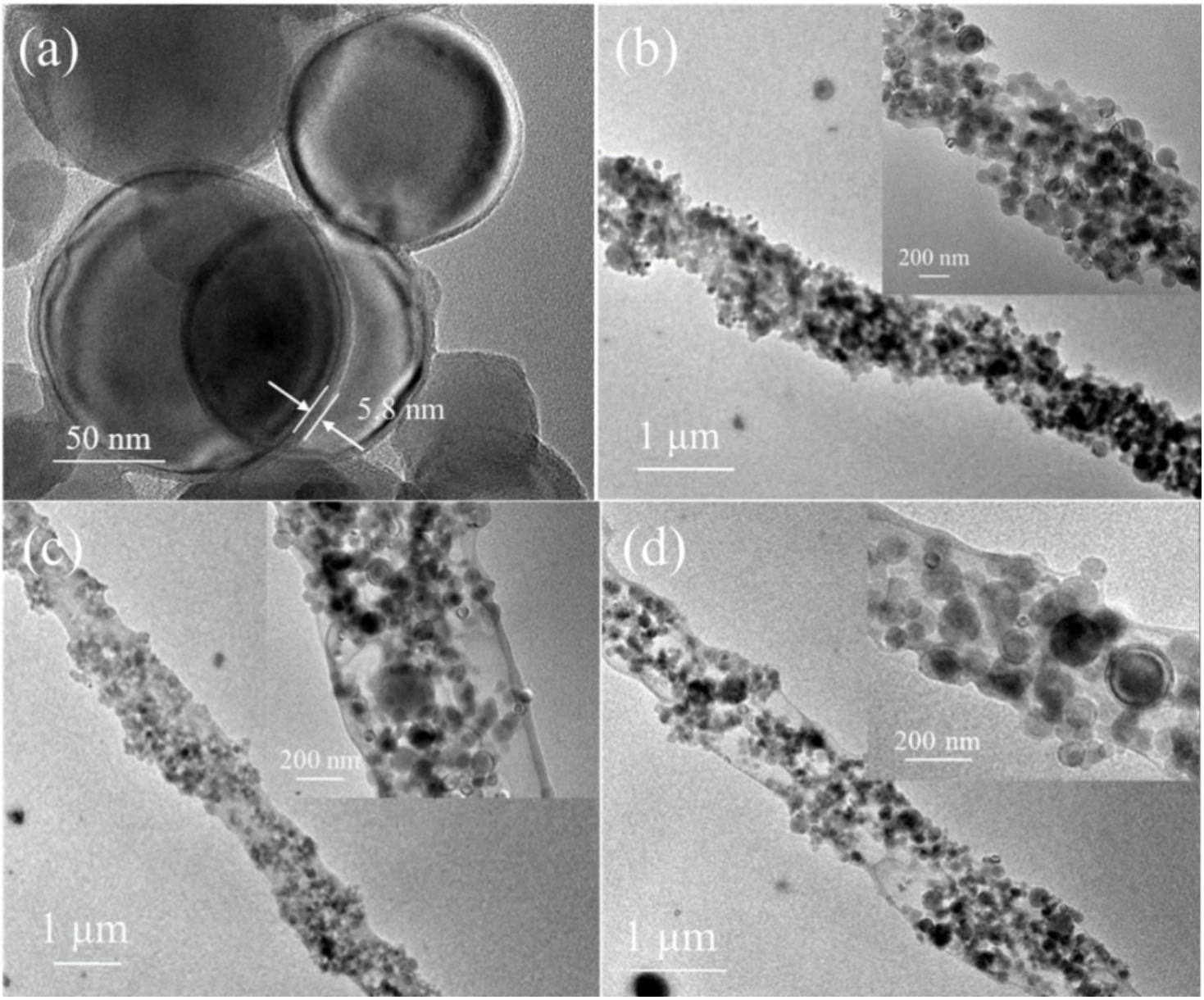

Figure 6

TEM images of nano Al particles (a) and NC/Al composite fibers with different mass ratio of NC to Al: (b) 1:1, (c) 3:1, (d) 5:1.

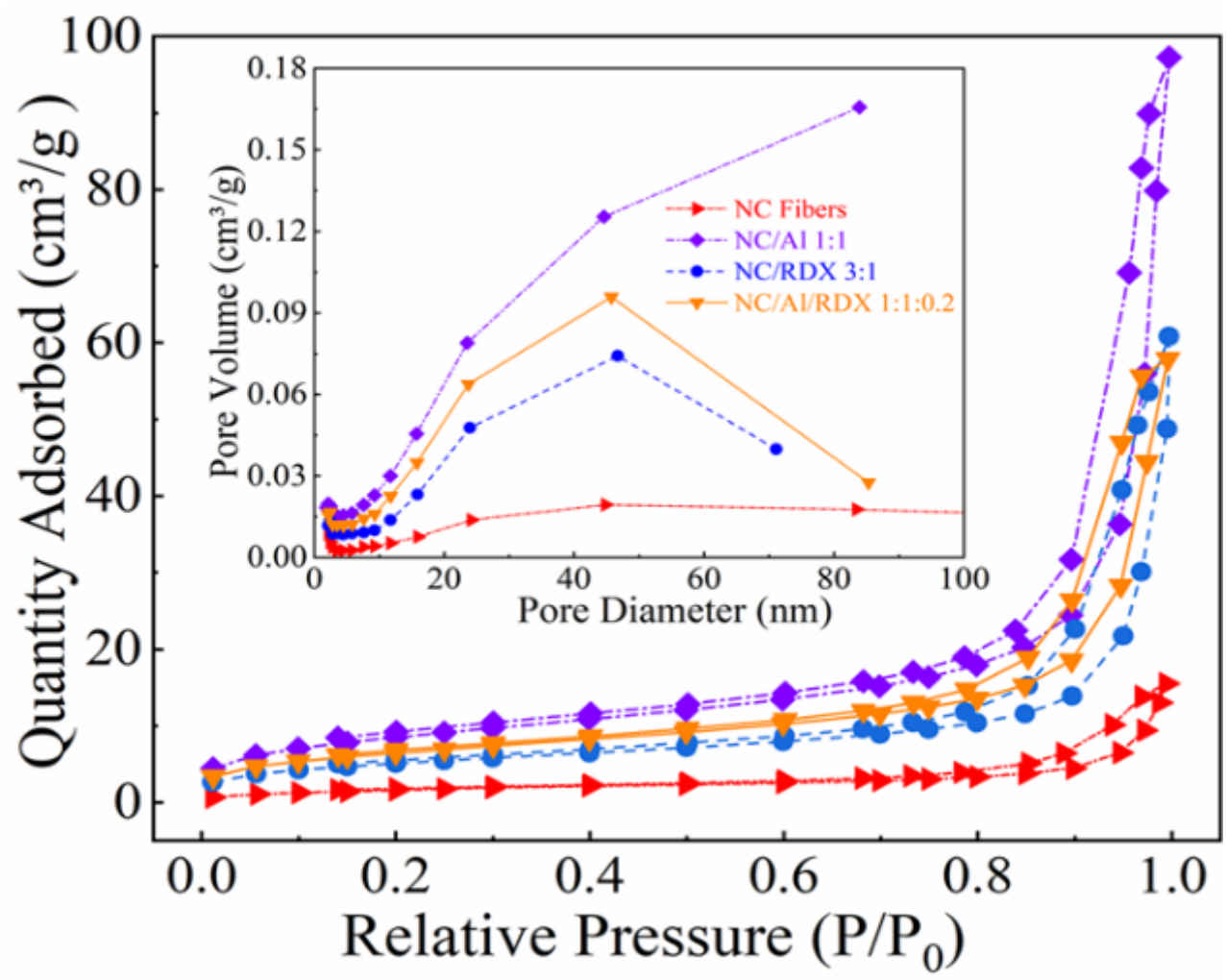

Figure 7

Nitrogen adsorption-desorption isotherms of NC, NC/Al, NC/RDX and NC/Al/RDX composite fibers. Inset: the pore size distribution of the corresponding samples.

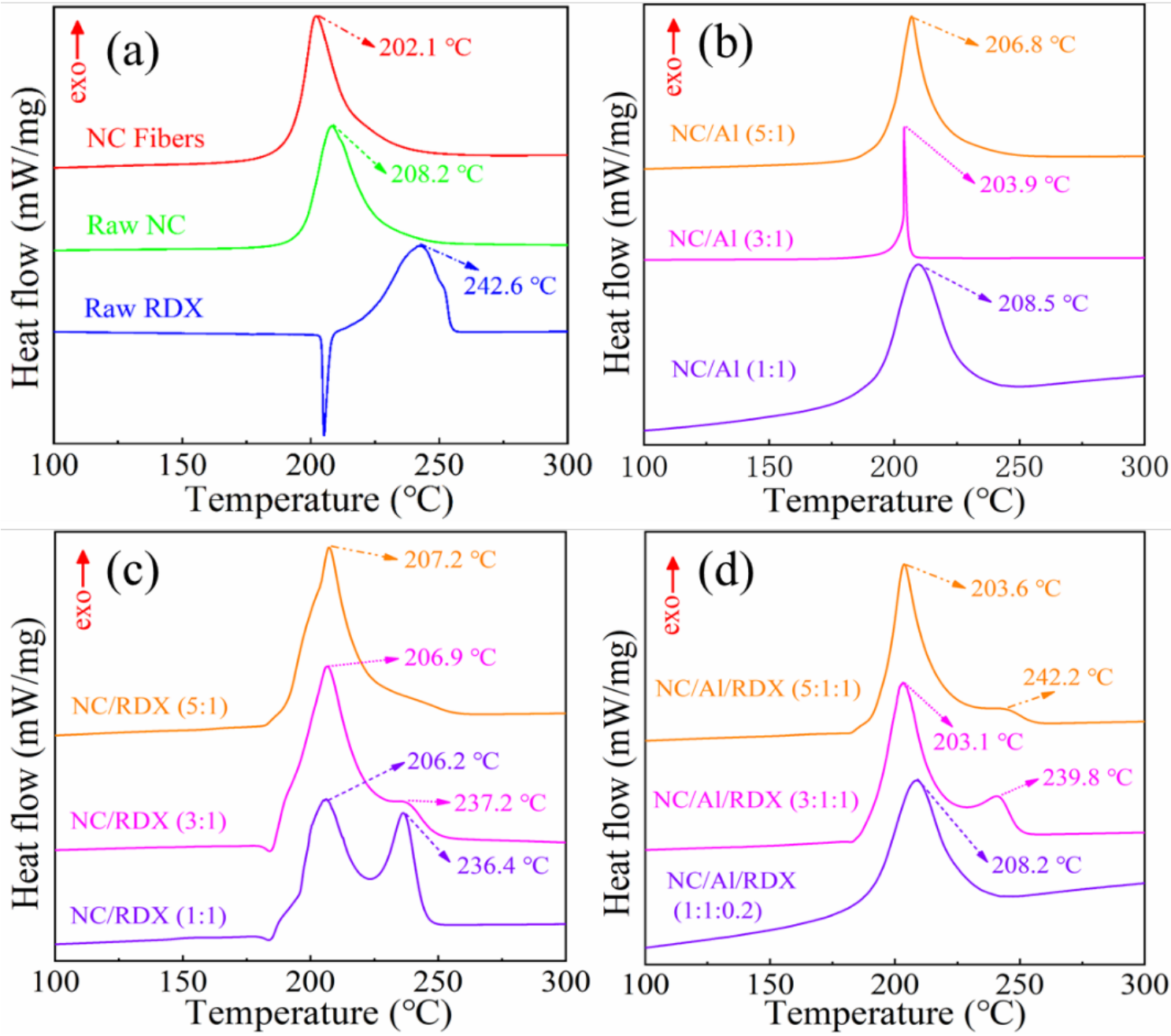

Figure 8

The DSC curves of (a) NC Fibers, NC and RDX, (b) NC/Al, (c) NC/RDX and (d) NC/Al/RDX at 10 °C min-1 under N2 flow.

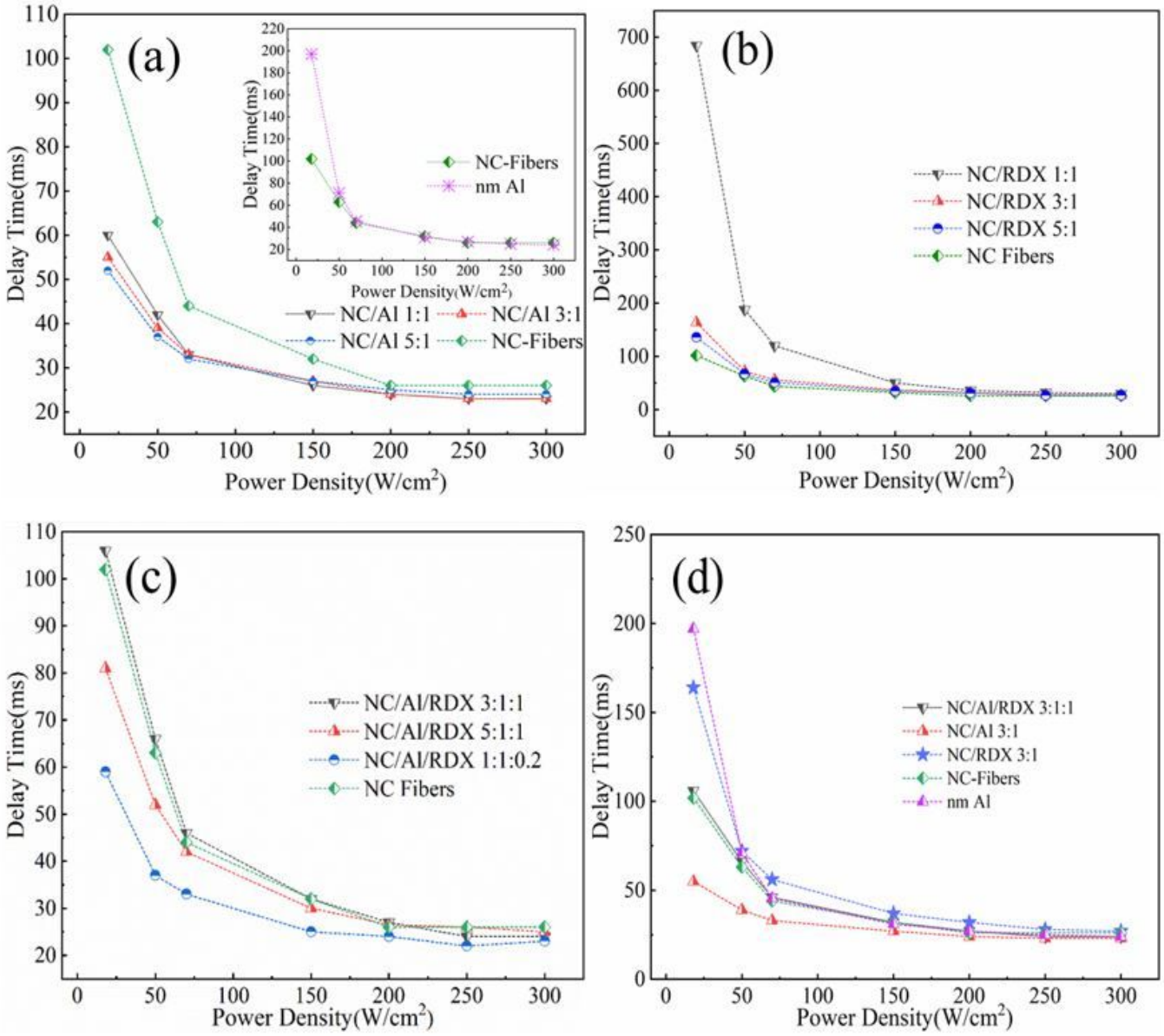

Figure 9

The ignition delay time changing with the laser power density for all the samples in the air: (a) NC/Al, (b) NC/RDX, (c) NC/Al /RDX and (d) their comparison

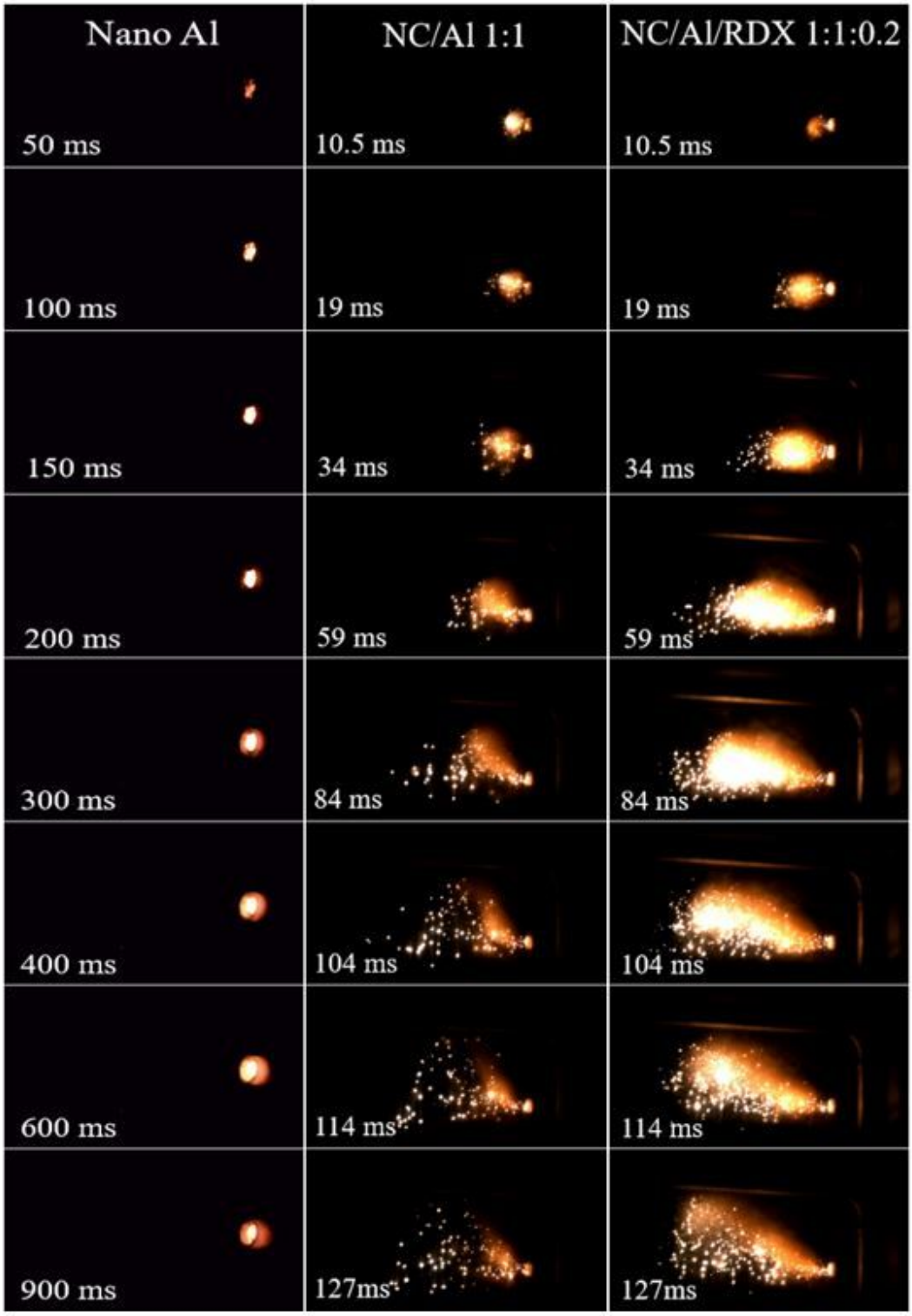

Figure 10

The burning snapshots of the nano-Al, NC/Al (1:1), and NC/Al/RDX (1:1: 0.2) in air atmosphere. Note: The time stamps on the top of each image indicate elapsed time.